Towards a programmable magnetic bead microarray in a microfluidic channel

Kristian Smistrup, Henrik Bruus, Mikkel F. Hansen*

MIC—Department of Micro and Nanotechnology, Technical University of Denmark, DTU, Building 345 East, DK-2800 Kongens Lyngby, Denmark

Available online 19 December 2006

Abstract

A new hybrid magnetic bead separator that combines an external magnetic field with 175 µm thick current lines buried in the back side of a silicon wafer is presented. A microfluidic channel was etched into the front side of the wafer. The large cross-section of the current lines makes it possible to use larger currents and obtain forces of longer range than from thin current lines at a given power limit. Guiding of magnetic beads in the hybrid magnetic separator and the construction of a programmable microarray of magnetic beads in the microfluidic channel by hydrodynamic focusing is presented.
© 2006 Elsevier B.V. All rights reserved.

Keywords: Magnetic microsystems; Magnetic separation; Magnetic bead; Programmability; Microarray; Lab on a chip

1. Introduction

Magnetic manipulation of magnetic beads in microfluidic channels is receiving growing attention in the literature due to its high potential for use in bioanalysis in lab-on-a-chip systems [1,2]. Recently, several reports have appeared on the creation of arrays of magnetic beads in microfluidic channels [3–5]. Conventional microarrays in lab-on-a-chip systems are usually constructed by micro-contact printing during the fabrication process. While this process allow for many array spots, these arrays are static and single-use. When the array is constructed from differently functionalized magnetic beads addressed to specific capture sites, a dynamic array is achieved that is potentially reusable. This makes the system fabrication and use more flexible as several assays can be performed in the same portable microsystem simply by changing the functionalization of the beads [5]. For example, a medical doctor may be able to acquire beads functionalized with antibodies for a new strand of the flu, and with the microsystem and a microscope, she can perform assays testing for the new strand as well as older ones on the patient sample while the patient is still in the office. With conventional methods, a new system would have to be made as the spotting takes place during the fabrication. Bead manipulation has been carried out using active systems with on-chip electromagnets [6–9], passive systems where on-chip magnetic structures are magnetized by an external magnetic field [5], and hybrid systems where on-chip current lines work in combination with an applied external magnetic field [10–12]. Large magnetic forces are achievable in the passive systems, but these lack addressability of the individual capture sites. The systems with active electromagnetic structures are addressable but the forces are typically small and short-range. Furthermore, the large currents needed to achieve sufficient forces for capturing beads typically lead to hot spots, which may interfere with the biology in the channels.

Here, we present and demonstrate a new design, shown in Fig. 1, for creating arrays of magnetic beads in a microfluidic channel. The design is based on on-chip current lines combined with an external magnetic field and hydrodynamic focusing of a stream of beads. The 175 µm thick current lines are buried in the back side of a silicon wafer in which the fluidic channel is etched into the front side. This is different from previous reports in the literature where the current lines are structured in a 0.1–0.3 µm thick film at or near the channel bottom [10–13]. Due to the larger cross-section of the buried

*Corresponding author. Tel.: +45 4525 6338; fax: +45 4588 7762.
E-mail address: mfh@mic.dtu.dk (M.F. Hansen).
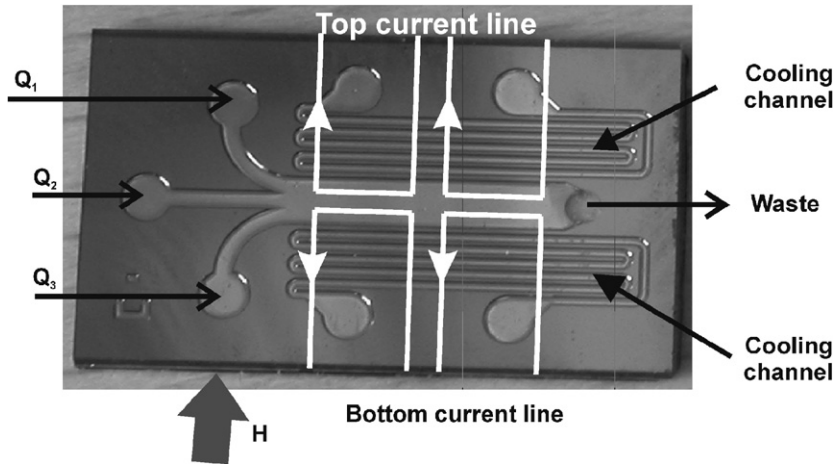
Fig. 1. Top view of channel side of microsystem. The channel has three inlets 1, 2, and 3 with flow rates Q_1, Q_2, and Q_3, respectively. The channel has length × width × depth = $8500 \times 1500 \times 100 \, \mu m^3$. The outlet is through the bottom of the wafer. Cu current lines with $t \times w = 175 \times 20 \, \mu m^2$ are buried in the back side of the wafer at the positions indicated by the white lines. An external magnetic field is applied across the chip as indicated. Also included on the chip is a set of channels for cooling by heat-exchange with a coolant.

current lines, they can sustain a larger current at a given power limit. Moreover, heat is efficiently dispersed due to the high thermal conductance of the silicon wafer, which can also contain microfluidic channels for a coolant. We show that the resulting magnetic forces are of longer range than when the current lines are fabricated in thin films on the channel bottom and demonstrate the construction of arrays of different types of magnetic beads within a microfluidic channel by this approach.

2. Theory and microsystem design

The magnetic force, $\mathbf{F}_{mag}$, on a bead is

$$\mathbf{F}_{mag} \cong \mu_0 V_{bead} (\mathbf{M}_{bead} \cdot \nabla) \mathbf{H}_0, \tag{1}$$

where μ_0 is the permeability of free space, V_{bead} the volume of a bead, $\mathbf{M}_{bead}$ the magnetization of the magnetic bead calculated at the bead center, and $\mathbf{H}_0$ the applied magnetic field present in the absence of the bead calculated at the centre of the bead. The force on a bead in a non-magnetic medium is directed towards field maxima. To maximize this force, the bead must be magnetically saturated, and the gradient of the magnetic field must be as large as possible.

Below, we assume that the bead magnetization is saturated along the external magnetic field, and thus we only consider the magnitude of the field gradient. We consider the field and current line geometry sketched in Fig. 1. This configuration allows for both attractive and repulsive forces near the current lines. When the current is applied in the indicated positive direction, the magnetic field from the current line adds to the external field and creates a local field maximum over the line to which the beads are attracted. A current applied in the opposite direction leads to a repulsive force.

The power, P, dissipated in a current line is $P = I^2 R$, where I is the current, and $R = \rho L (tw)^{-1}$ is the resistance of the wire, where ρ is the material resistivity, L is the length

of the wire, t is the thickness, and w is the width of the wire. Using the definitions of P and R, we obtain $I = (Pwt)^{1/2} (\rho L)^{-1/2}$. We now consider the magnitude of the magnetic field above the middle of a current line. Denoting the distance from the channel bottom to the bead r and the distance from the top of the current line to the channel bottom r_0, the magnitude of the magnetic field is approximately $H(r) \approx I[\{2\pi(r + r_0) + 2t + 2w\}]^{-1}$ (Ampére's law). Inserting I and taking the gradient, we find

$$\left| \nabla H(r) \right| \approx \frac{C\sqrt{t}}{(2\pi(r + r_0) + 2t + 2w)^2} \tag{2}$$

with $C = 2\pi (Pw)^{1/2} (\rho L)^{-1/2}$. For a fixed power and geometry ($w = 20 \, \mu m$), we now compare a system with $t_1 = 0.3 \, \mu m$ and $r_{0,1} = 1 \, \mu m$ representing a thin film current line at the bottom of a channel with one with $t_2 = 175 \, \mu m$ and $r_{0,2} = 50 \, \mu m$ representing a thick current line of the present study. The simple approximation in Eq. (2) predicts that the ratio of the field gradient due to the thick current line to that due to the thin current line is $(t_2/t_1)^{1/2} [\{2\pi(r + r_{0,1}) + 2t_1 + 2w\}/\{2\pi(r + r_{0,2}) + 2t_2 + 2w\}]^2$. At the channel bottom ($r = 0$) and top ($r = 100 \, \mu m$), respectively, it predicts the ratios 0.1 and 6. The ratio is larger than 1 for r larger than $19 \, \mu m$. A numerical calculation by the method outlined below yields the ratios 0.4 and 10 at the bottom and top of the channel, respectively, and that the ratio is greater than 1 for r larger than $15 \, \mu m$ in reasonable agreement with the approximate model. Hence, a significantly larger force is achievable at the channel bottom by use of the thin current lines, but this force is of shorter range and acts locally. A thick current line can provide strong field gradients of longer range than the thin current lines and thus seems to be a better choice for the capture of magnetic beads in typical microfluidic channels.

The choice of geometry in the present work was based on simulations and fabrication limitations. Each current line

sketched in Fig. 1 has a cross section of $t \times w = 175 \times 20 \, \mu m^2$ and it is placed at a spacing of $50 \, \mu m$ to the channel of length $\times$ width $\times$ depth $= 8500 \times 1500 \times 100 \, \mu m^3$. The current lines were placed in pairs of two with a centre-to-centre spacing of $750 \, \mu m$.

We find the magnetic field $\mathbf{H} = \mu_0^{-1} \nabla \times \mathbf{A}$ using the finite element method in Comsol Multiphysics 3.2a and solve the differential equation

$$\mu_0^{-1} \nabla \times \nabla \times (A_z \hat{\mathbf{z}}) = J_z \hat{\mathbf{z}},$$

where J_z is the current density in the z-direction, and A_z is the z-component of the magnetic vector potential, $\mathbf{A}$. The outline of the simulation geometry is sketched in Fig. 2. The shown (left) boundary has the condition $\mathbf{n} \times \mathbf{H} = \mathbf{0}$, where $\mathbf{n}$ is a boundary normal vector, since the magnetic field must be perpendicular to this boundary due to symmetry. The other boundaries are far away, and subject to the condition $A_z = \mu_0 H_0 y$, where y is the vertical coordinate and H_0 is the magnetic field applied in the horizontal direction.

We now compare the magnetic force on a MyOne magnetic bead to the buoyancy force. The beads have the diameter $d_{bead} = 1.05 \, \mu m$, the mass density $\rho_{bead} = 1.7 \, g/cm^3$, the saturation magnetization $M_s = 39950 \, A/m$, and the initial susceptibility $\chi_0 = 1.377$ (SI) [14]. With these numbers, the downwards buoyancy force is

$F_{buoy} = V_{bead}(\rho_{bead} - \rho_{water})g = 4.2 \times 10^{-15} \, N$, where g is the gravitational acceleration. The magnetic force is found from Eq. (1) with $|\mathbf{M}_{bead}| = M_s L(3\chi_0 |\mathbf{H}|/M_s)$, where L is the Langevin function. Fig. 2 shows the magnitude of the magnetic force field on a MyOne magnetic bead calculated in an external magnetic field of $50 \, kA/m$ with a current of $2 \, A$ through the current line. The arrows show the direction of the force field, the greyscale chart and the contour lines show the base 10 logarithm of the magnetic force divided by the buoyancy force. For example, within the 2.0 contour, the magnetic force is more than 100 times the buoyancy force. The situation below the current line is equivalent to reversing the current showing that a repulsive force can be obtained.

3. Experimental

3.1. Microsystem fabrication

The microsystem was fabricated using cleanroom technology. The labels below refer to Fig. 3, which schematically illustrates a cross-section of a chip during fabrication. (a) A $2.45 \, \mu m$ thick oxide is grown on a double-polished $350 \, \mu m$ thick Si wafer. (b) The fluid channels are defined in the oxide on the front side using
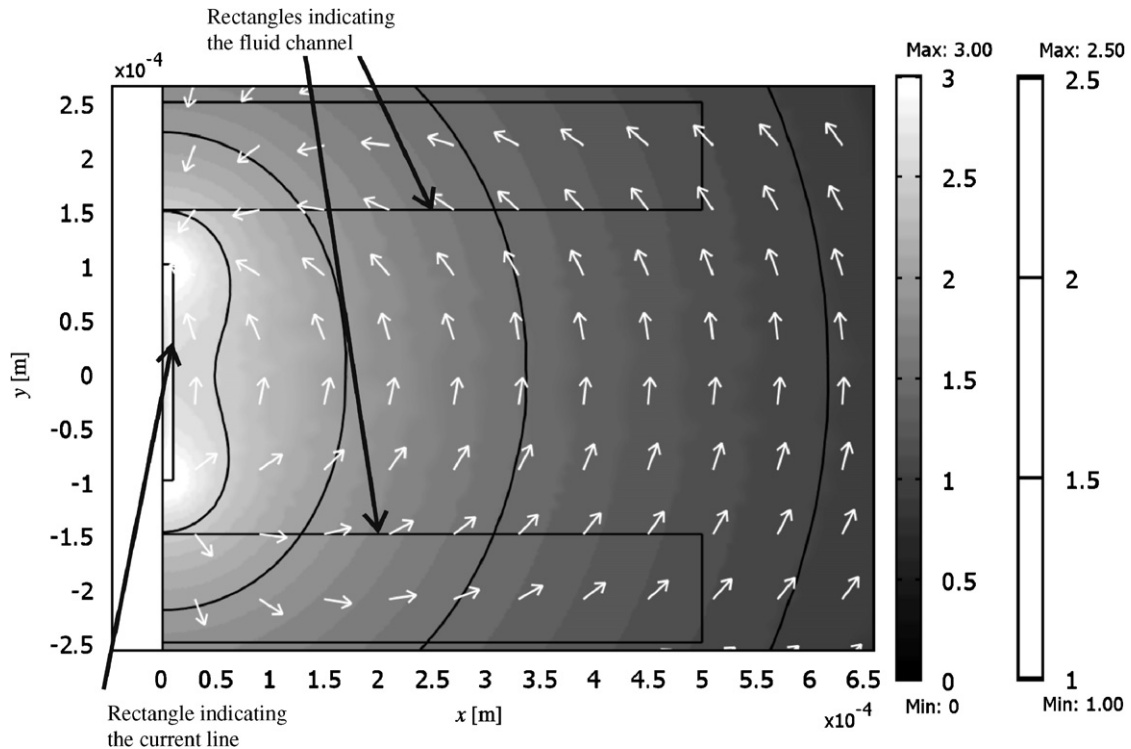
Fig. 2. Result of finite element calculation of the magnetic force field on a MyOne magnetic bead near a current line carrying a current of $2 \, A$ in an external field of $50 \, kA/m$ applied in the horizontal direction. The outlines of the current line and the channel are indicated in black. The channel is shown both above and below the current line. The force field above corresponds to the situation where the external field and the field from the current line couples constructively. That below corresponds to a situation, where the current is reversed, and repulsive forces are generated. Due to symmetry, only half of the geometry is considered. The arrows show the direction of the magnetic force. The gray scale and contour plots show the base 10 logarithm of the magnetic force over the buoyancy force on the scales shown to the right of the graph.
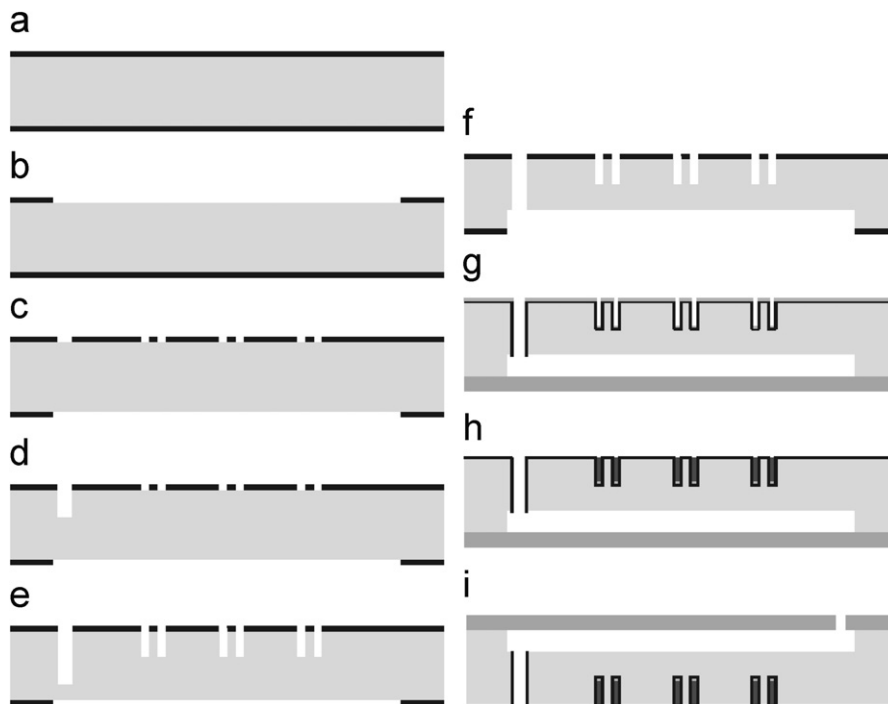
Fig. 3. Schematic illustration of a chip cross-section during the cleanroom fabrication described in the text.

photolithography and oxide etch in buffered HF. (c) The current lines and the through-hole for the fluid outlet are defined in the oxide on the back side. (d) Using a third photoresist mask, the through-hole is etched using deep reactive ion etching (DRIE) to a depth of approximately 130 μm. (e) After resist strip, the trenches for the current lines are etched using DRIE to a depth of 200 μm using the oxide as a mask. (f) The fluidic channels are etched to a depth of 100 μm using DRIE. During the etching, the wafer is temporarily bonded to a handle wafer as the through-hole is etched all the way through the wafer. (g) An RCA-clean is performed, a 1.2 μm thick oxide is grown, the oxide is removed on the fluid side, a pyrex wafer is bonded anodically to the fluid side, and a seed layer of 5/200 nm Ti/Au is deposited using e-beam evaporation on the current line side. E-beam evaporation gives poor step coverage and thus poor or no electrical contact between the Au on top of the wafer and that in the bottom of the trenches. (h) A series of short Au etches are performed using Entreat (Engelhard, NJ, USA) until the resistance between the top and bottom of the wafer back side with the current lines is larger than 250 kΩ. Then, a 2.5 μm thick Cu layer is electroplated in the bottom of the trenches using a CuproStar LP-1 electrolyte (Enthone, CT, USA). The mask is designed such that all trenches for the current lines are connected to the rim of the wafer. Using the Cu as etch mask, the remaining uncovered Au is removed in an Au etch. Then Cu is electroplated to a total thickness of 175 μm using the same electrolyte as before. (i) Fluid inlets are drilled through the pyrex wafer using a diamond drill.

3.2. Experimental setup

For the experiments, the chips were mounted in a chip-holder with O-ring sealed fluidic connections. Electrical contact to the current lines was established by soldering. The currents and the numbering of the inlets and liquid flows refer to Fig. 1. The bead solution was infused through inlet 2 and the buffer solution (milli-Q water) was infused through inlets 1 and 3 by use of three syringe pumps. Electrical currents I_{top} and I_{bottom} could be applied to the top and bottom current lines, respectively. Pictures were taken using a Leica MZ FL III microscope equipped with a Sony DFW-X710 CCD camera and FITC fluorescence filters. A homogeneous magnetic field of 50 kA/m was supplied by permanent magnets mounted in a soft iron frame.

3.3. Bead guiding experiments

Eight micron FITC-fluorescent magnetic beads (FCM-8052-2, Spherotech, Inc.) were used for the demonstration of bead focusing and guiding experiments. The solution supplied from the manufacturer was diluted with milliQ water to 20 μg/mL. The bead solution was infused at $Q_2 = 2 \mu L/min$ (buffer: $Q_1 = Q_3 = 0$). A current of $I_{top} = I_{bottom} = 2 A$ was applied to the current lines. Pictures were taken with a FITC-filter, and an exposure time of 9 s.

3.4. Magnetic bead microarray experiments

First, the bead capturing capability of the system was tested with 2 A through all current lines and 1 μm magnetic

bead solution with 20 μg/mL (MyOne, Invitrogen) flowing at $Q_2 = 2$ μL/min and no buffer flows ($Q_1 = Q_3 = 0$). Then, the capability to create arrays of different types of beads was demonstrated. Two types of beads were used for these experiments: 1 μm non-fluorescent magnetic beads (MyOne, Invitrogen) and 1 μm FITC-fluorescent magnetic beads (FCM-1052-2, Spherotech). All bead solutions were diluted with milliQ water to 20 μg/mL. The procedure was as follows: (1a) With $I_{bottom} = 2.5$ A and $I_{top} = 0$, MyOne bead solution was infused at $Q_2 = 10$ μL/min for 2 min (buffer: $Q_1 = 10$ and $Q_3 = 0$ μL/min), such that the bead solution is hydrodynamically focused at the side of the channel at the bottom of Fig. 1. (1b) The flow rates were then lowered to $Q_2 = 0.7$ μL/min and $Q_1 = 1.5$ μL/min for 15 min to facilitate the capture of the hydrodynamically focused magnetic beads at the bottom current lines. (1c) The non-fluorescent MyOne beads remaining in the inlet tubes were then flushed out and through the channel by buffer at $Q_2 = 3$ and $Q_1 = 3$ μL/min for 5 min. (2a) Currents of $I_{bottom} = I_{top} = 2.5$ A were applied and the fluorescent Spherotec bead solution was infused at $Q_2 = 3$ μL/min for 5 min (buffer: $Q_3 = 3$ μL/min and $Q_1 = 0$), such that the bead solution was now hydrodynamically focused at the side of the channel at the top of Fig. 1. (2b) Again, the flow rates were lowered to $Q_2 = 0.7$ μL/min and $Q_3 = 1.5$ μL/min for 15 min. Micrographs were recorded with and without FITC-fluorescence filters to demonstrate the successful construction of the bead array.

4. Results and discussion

4.1. Bead guiding experiments

Fig. 4 shows fluorescence micrographs taken with long exposure time during the capture of 8 μm fluorescent magnetic beads. In the figure, the trajectories of individual beads are traced during the exposure. It is clearly seen that the beads are guided towards the current lines. Close to the current lines, the beads slow down and finally settle at the bottom of the channel. This demonstrates the bead focusing due to the current lines and that the system is able to capture 8 μm magnetic beads.

4.2. Magnetic bead microarray experiments

First, we present the demonstration of the bead capturing capability of the system. Fig. 5(a) shows a micrograph after 1 μm MyOne magnetic beads have been introduced into the entire channel. It is clearly seen that the beads are captured at the top of the current lines in the channel, whereas essentially no beads are present elsewhere in the channel. This shows the ability of the system to capture 1 μm magnetic beads and illustrates the attraction of the beads towards the current lines. Moreover, it should be noted that the beads are evenly distributed along each current line. This makes the surface of the bead agglomerates large and hence more available for biochemical reactions. In the greyscale micrographs in Figs. 5(a) and (b) not only the captured beads are visible, but also some spurious dots. The latter are either dust from the drilling process or freely flowing beads, neither of which show up on a fluorescence micrograph, such as Fig. 5(c).

Now, we turn to the demonstration of the construction of a magnetic bead microarray. Experiments in which 1 μm fluorescent and non-fluorescent magnetic beads were placed at the top and bottom of the images of the channel were carried out as described in the experimental section. Figs. 5(b) and (c) show a normal micrograph and a fluorescence micrograph, respectively, of the same section of the microfluidic channel. In the normal micrograph, two lines of beads are situated on top of the current lines
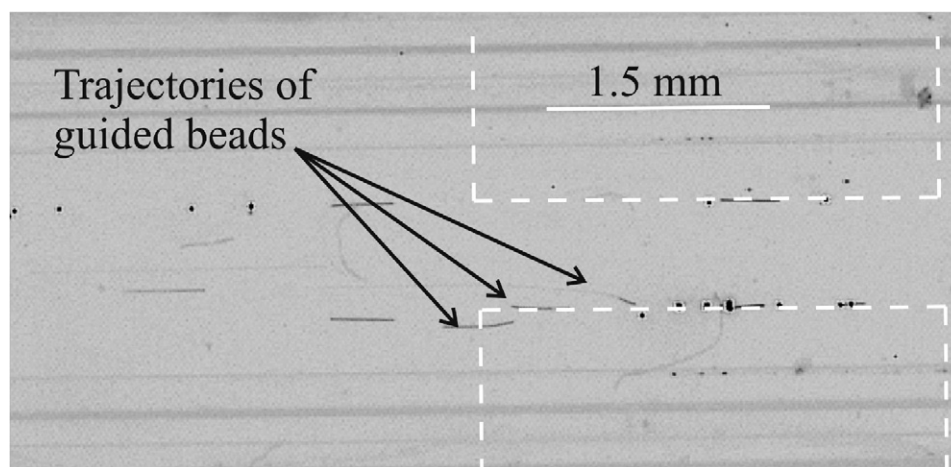
Fig. 4. Fluorescence micrograph illustrating magnetic beads being guided towards current lines and captured. The original image has been converted to greyscale, inverted, and some color/sharpness adjustments have been made. The long exposure time allows tracking of individual 8 μm beads in the microfluidic channel. The darker the bead trajectory, the slower the bead moves. The white dotted lines indicate the position of the current lines on the backside of the wafer.
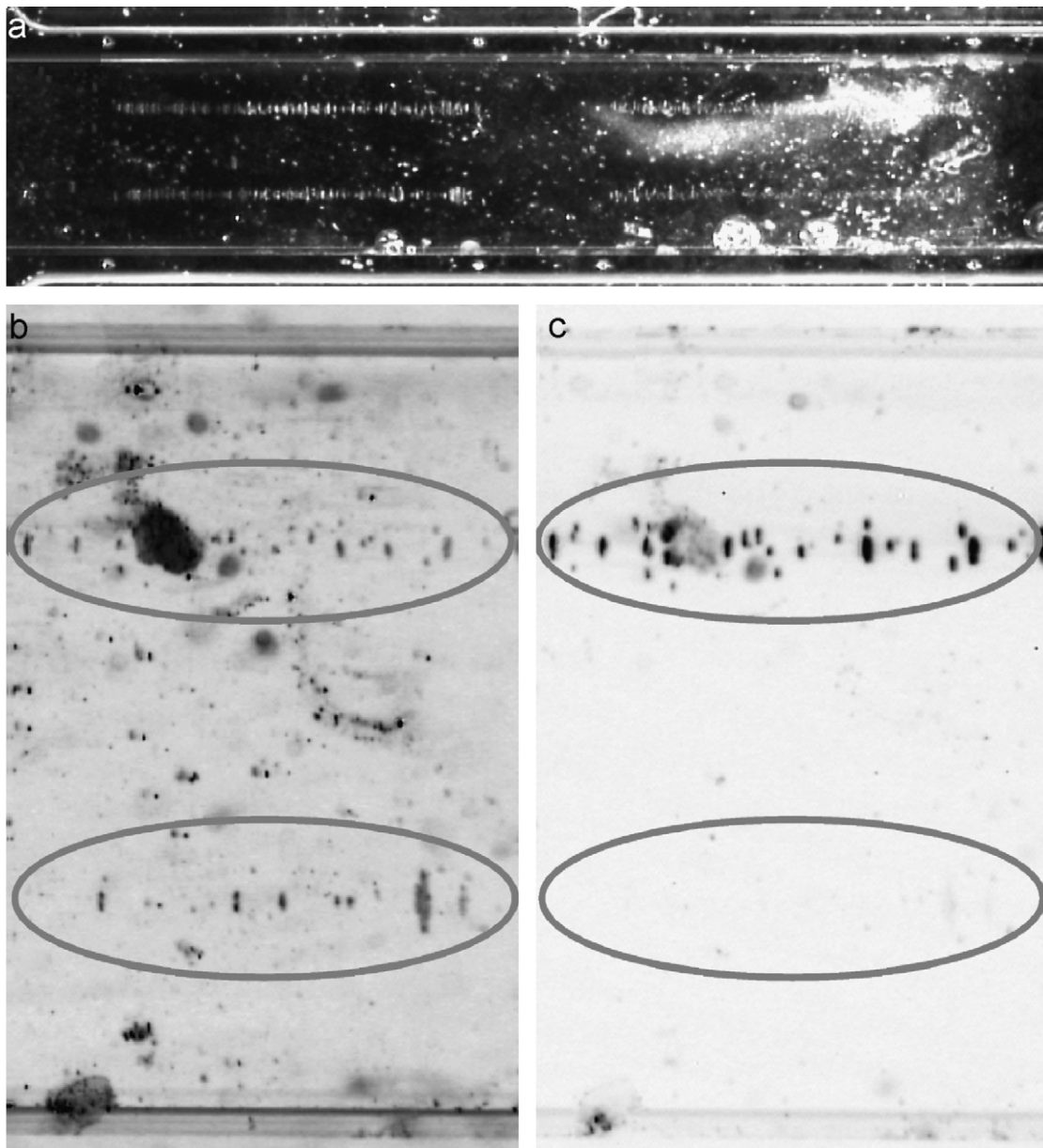
Fig. 5. (a) Micrograph of MyOne beads captured on all four current lines. In (b) and (c) fluorescent and non-fluorescent magnetic beads are captured at the top and bottom current lines as described in the text. The close-ups in (b) and (c) show a micrograph and a fluorescence micrograph of the same section of the channel, respectively. The colors have been inverted in both (b) and (c). Both types of beads are seen in (b), whereas in (c) only the fluorescent beads are observed. The width of the microfluidic channel in all images is 1.5 mm.

(encircled), whereas in the fluorescence micrograph only one line of beads is observable (encircled). This shows that it is possible to selectively place beads at each of the current lines with no cross-talk by combining hydrodynamic focusing of the beads and the guiding of each current line.

During the experiments, it was noted that beads were not only captured at the first current line but also at the current line further down the channel. Bead trajectory simulations, performed using the methods described by Smistrup et al. [15], indicated that all beads should be captured at a single current line. This difference is most likely due to the fact that the holding force (the force opposing the liquid flow) on the beads along the channel direction is weak such that

they tend to roll along with the liquid flow. Furthermore, the simulations only deal with the capture of a single bead and the influence of beads that are already captured is neglected. Finally, the syringe pump introduces a slightly pulsating flow, which tends to tear captured beads loose. Air bubbles in the fluidic setup can also cause pulsations in the fluid pressure. These facts make it difficult to create arrays of beads at sites along the length of the channel, which are at the same position along the width of the channel.

We have previously reported on other designs of array systems [4,5]. The hybrid system of the present paper is clearly superior to the active system presented in Ref. [4];

the hybrid system has the same addressability, more capture sites, create larger magnetic forces, and it is easier to fabricate. Compared to the passive system in Ref. [5], the hybrid system has the potential for more capture sites, the beads are spread out along the channel bottom instead of being captured on the channel sidewall, it is addressable, but it creates smaller magnetic forces. Here the magnetic forces have not been measured, but they have been calculated in Comsol Multiphysics for all three systems.

5. Conclusion

We have demonstrated a new design of a hybrid magnetic separator where thick current lines are fabricated in trenches etched into the back side of a silicon wafer and a fluidic channel is etched into the front side. Simple theoretical considerations show that this procedure significantly increases the range of the magnetic force compared to thin current lines. Hence, by this approach the range of the magnetic force of hybrid magnetic separators is extended to length scales that are relevant for lab-on-a-chip applications. The integration of the current lines into the silicon wafer, which is a good heat conductor, makes it possible to efficiently disperse the generated heat and channels for a coolant are also easily integrated.

We have demonstrated the use of the new hybrid magnetic separator design for guiding and capturing magnetic beads as well as for the selective placement of two different types of magnetic beads at the bottom of a microfluidic channel in a hybrid magnetic separator by use of hydrodynamic focusing. This is the prerequisite for creating an array of different types of magnetic beads at the bottom of the channel and the method is expandable to more than two types of beads.

Acknowledgments

References

[1] M.A.M. Gijs, Microfluid. Nanofluid. 1 (2004) 22.
[2] N. Pamme, Lab Chip 6 (2006) 24.
[3] B.B. Yellen, G. Friedman, Lab Chip 20 (2004) 2553.
[4] K. Smistrup, O. Hansen, P.T. Tang, et al., in: Proceedings of the MicroTAS 2004, Malmö, Sweden 1 (2004) 509.
[5] K. Smistrup, B.G. Kjeldsen, J.L. Reimers, et al., Lab Chip 5 (2005) 1315.
[6] J.W. Choi, T.M. Liakopoulos, C.H. Ahn, Biosens. Bioelec. 16 (2001) 409.
[7] R. Rong, J.W. Choi, C.H. Ahn, in: Proceeding of the MEMS 2003, Kyoto, Japan, IEEE, Piscataway, NJ, 2003, p. 530.
[8] C.S. Lee, H. Lee, R.M. Westervelt, Appl. Phys. Lett. 79 (2001) 3308.
[9] K. Smistrup, P.T. Tang, O. Hansen, et al., J. Magn. Magn. Mater. 300 (2006) 418.
[10] M. Tondra, M. Granger, R. Fuerst, et al., IEEE Trans. Magn. 37 (2001) 2621.
[11] A. Rida, V. Fernandez, M.A.M. Gijs, Appl. Phys. Lett. 83 (2003) 2396.
[12] T. Deng, G.M. Whitesides, M. Radhakrishnan, et al., Appl. Phys. Lett. 78 (2001) 1775.
[13] A. Ramadan, V. Samper, D. Poenar, et al., J. Magn. Magn. Mater. 281 (2004) 150.
[14] G. Fonnum, C. Johansson, A. Molteberg, et al., J. Magn. Magn. Mater. 293 (2005) 41.
[15] K. Smistrup, O. Hansen, H. Bruus, et al., J. Magn. Magn. Mater. 293 (2006) 597.